International Journal of Modern Physics A


# First results from the MEG experiment: $\mu^+ \to e^+\gamma$

Paolo Walter Cattaneo on behalf of the MEG collaboration
*INFN Pavia, Via Bassi 6,*
*Pavia, I-27100, Italy, paolo.cattaneo@pv.infn.it*

The MEG collaboration has performed a search for the decay $\mu^+ \to e^+\gamma$ based on $\approx 10^{14}$ $\mu^+$ stopped on target during 2008 by means of a superconducting spectrometer and a large liquid xenon calorimeter. The search yields an upper limit $BR(\mu^+ \to e^+\gamma) \leq 2.8 \times 10^{-11}$ (90% C.L.).

*Keywords*: Muon decay, lepton flavor violation

PACS numbers: 13.35.Bv, 11.30.Hv

## 1. Introduction

The MEG experiment, operating at the 590MeV proton cyclotron at the Paul Scherrer Institut (PSI), in Switzerland has collected $\approx 10^{14}$ $\mu^+$ on target during the 2008 run, to study the lepton flavor violating decay $\mu^+ \to e^+\gamma$. Exact lepton flavor violation (LFV) in the Standard Model (SM) is dependent on neutrinos being massless. Neutrino oscillation phenomenology Ref 1 implies that the neutrinos have non-zero masses, but that they are so small that their contribution to LFV processes are many order of magnitude below experimental reach. In extensions of SM, LFV rates may become much larger Ref 2-3 and experimentally accessible. Hence improving existing experimental bounds, especially on the $\mu^+ \to e^+\gamma$ channel, often the most sensitive to new physics, is of great relevance to investigate these extensions.

## 2. The Experimental principle

The decay $\mu^+ \to e^+\gamma$ is a two-body final state, with the $e^+$ and $\gamma$ coincident in time and origin. In the rest frame of the $\mu^+$, the particle momenta are opposed in sign, each with an energy equal to half the $\mu$ mass.
The background sources are mainly from the radiative decay $\mu^+ \to e^+\nu_e\overline{\nu}_\mu\gamma$ (RMD) and from accidental coincidences between a $e^+$ close to the kinematic limit from $\mu^+ \to e^+\nu_e\overline{\nu}_\mu$ (Michel decay) and a high energy $\gamma$ from RMD, $e^+$ annihilation in flight or bremsstrahlung such that the two particles are moving in opposite directions. The latter source dominates in the MEG condition Ref 5.

### 2.1. *The MEG detector*

The whole apparatus is shown n Fig.2. Surface $\mu^+$ of 28 MeV/c momentum from the $\pi$E5 channel at PSI are stopped in a 205 $\mu m$ thick polyethylene/polyester target at the center of the magnet. The elliptical target is slanted with a 20.5° to the beam axis to provide sufficient stopping power to the $\mu^+$ and minimize material on the $e^+$ and $\gamma$ path. The $\mu^+$ stop rate is expected to be $3\times10^7\,\mu^+s^{-1}$ with minimal $e^+$ beam contamination. The target is positioned at the center of the COBRA (COnstant-Bending-RAdius) spectrometer consisting of a thin-walled superconducting magnet with a gradient magnetic field, a tracking system of low-mass drift chambers and two fast scintillator timing-counter arrays.

The gradient magnetic field in the spectrometer, ranging from 1.27 T at 0.49 T the ends, is designed such the $e^+$ bending radius is almost independent from the emission angle, so that the acceptance is higher for high momentum $e^+$ and sweeps away efficiently Michel $e^+$. The magnet bore is filled with He to minimize material

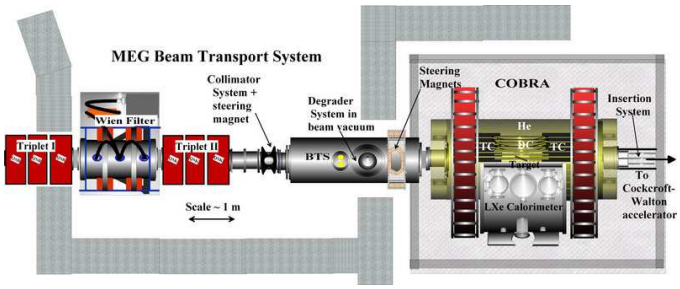


Fig. 1. MEG Beam Line, with the two sets of quadrupole triplet magnets on either side of the crossed-field separator (Wien filter). The superconducting transport solenoid (BTS) focuses the beam onto a degrader system. This degrader and the Helium-Air admixture inside COBRA slow-down the $\mu^+$ such that they stop in the target at the COBRA center.

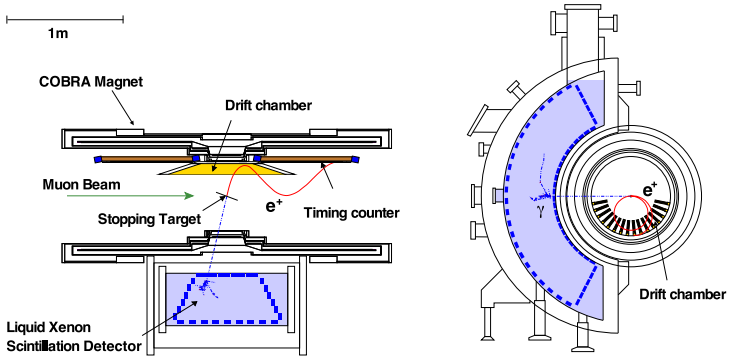


Fig. 2. COBRA positron spectrometer and LXe detector, showing the positron tracking chambers, the scintillator timing counter arrays and the superconducting gradient-eld solenoid COBRA.

for incoming and outgoing particles.

The drift chambers (DCH) consist of 16 radially aligned modules, spaced at 10.5° gap. Each DCH module has a trapezoidal shape with an open frame geometry with no support in the inner side to minimize the material. It has two staggered planes of nine drift cells filled with a He:$C_2H_6$ (50:50) gas. The two planes are separated and also enclosed by 12.5 m thick cathode foils with a Vernier pattern structure to measure the coordinate along the wire. The material of each module totals $2.5 \times 10^{-4} X_0$.

The $e^+$ timing is measured by a Timing Counter (TC) consisting of two sectors positioned at each end of the spectrometer. Each TC sector consists of an array of 15 BC404 fast scintillator bars and of 128 BFC-20 scintillating fibers placed orthogonally. Each bar is read-out at each end by a fine-mesh photomultiplier tube designed for operation in high magnetic field.

The calorimeter for $\gamma$ detection is a homogeneous liquid xenon (LXe) volume of 900 liters covering a solid-angle $\approx 10\%$. 846 PMTs detect the scintillation light to measure the energy, impact point and time of the $\gamma$. Liquid Xenon has the advantage of a fast response, large light yield and short radiation length.

The front-end signals are directed to both the trigger and the multi-GHz domino ring sampler chips (DRS), which record 1024 samples. The DCH signals are sampled at 500 MHz, while those of the PMTs from LXe and TC at 1.6 GHz. This approach allows to apply signal processing algorithm offline, to optimize time and amplitude resolution as well as pile-up rejection.

The trigger is fed with the waveforms sampled at 100 MHz and is based on information from the two fastest detectors: TC and LXe. The $\gamma$ is required to have energy close to 52.8 MeV and to be in coincidence in time and collinear with the $e^+$.

A detailed GEANT 3.21 based Monte Carlo simulation of the full apparatus (transport system and detector) has been used from the design and optimization phases to the calculation of acceptances and efficiencies.

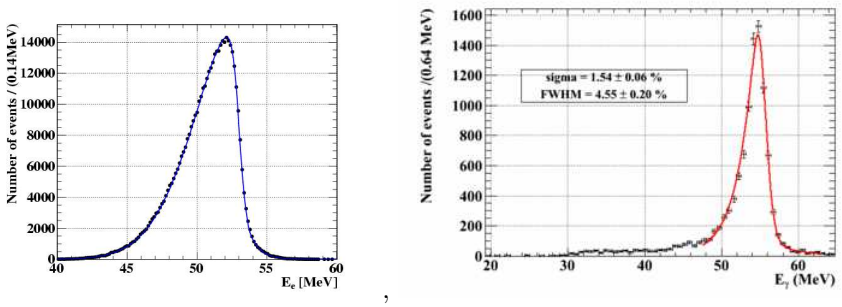


Fig. 3. Left: Positron energy. Right: Gamma Energy

### 2.2. *Monitoring and Calibration*

MEG performs high resolution measurements over a long time period, that requires continuous monitoring and frequent calibrations.
The most delicate items are the stability of the $\gamma$ energy measurement of the calorimeter and the relative timing between the DRS channels. The most important calibration tools are nuclear reactions from a Cockroft-Walton (CW) accelerator, radiative muon decays (RMD) and pion charge-exchange (CEX) reactions.
A dedicated CW-accelerator located downstream the detector is activated three times a week to accelerate protons with kinetic energy between 400 and 1000 keV onto a special $Li_2B_4O_7$ target. Photons with $E_\gamma = 17.67$ MeV are produced in $^7$Li(p,$\gamma$)$^8$Be to monitor the absolute energy scale of the calorimeter, while simultaneous $\gamma$'s from $^{11}$B(p,$\gamma$)$^{12}$C ($E_\gamma = 4.4, 11.6$ MeV) detected by the TC and the calorimeter determines the time offsets of TC bars.
Substantial amount of RMD data taken at reduced beam intensity allowed to determine the time offset between TC and calorimeter.
Using a dedicated $\pi^-$ beam on a liquid nitrogen target, the CEX reaction ($\pi^- p \to \pi^0 n \to \gamma\gamma n$) produced $\gamma$ pairs with $54.9 < E_\gamma < 83.0$ MeV. With a NaI calorimeter located opposite to LXe and an appropriate collimation, it was possible to obtain two monochromatic lines at the ends of the energy spectrum. That measured the energy scale and the uniformity. Dalitz decay ($\pi^0 \to \gamma e^+ e^-$) were used to study time synchronization and resolution betweem TC and LXe.

## 3. Event selection and resolutions

The data collected during 2008 amount to $\approx 10^{-14}$ $\mu^+$ on target. Data are prefiltered by requiring on track in the DCH and the LXe and TC Hit to be close in time. These data are further processed and those falling in a two dimensional window (blinding-box), centered around the $\gamma$ signal energy and relative time between the $\gamma$ and $e^+$ compatible with 0, are written separately. Only events outside the blinding-box are used to study the background and optimizing the analysis parameters.
During data taking, the DCH suffered an increasing loss in $e^+$ detection efficiency due to high voltage trips. This time varying efficiency was accounted for by adopting a normalization scheme insensitive to absolute efficiency and based on ratio between signal and Michel $e^+$ efficiency.
A candidate event is characterized by five kinematic parameters: $e^+$ energy ($E_e$), $\gamma$ energy ($E_\gamma$), relative time between $e^+$ and $\gamma$ ($t_{e^+\gamma}$) and angles between the two particles ($\theta_{e^+\gamma}$ and $\phi_{e^+\gamma}$).

### 3.1. *The positron energy $E_{e^+}$*

The $e^+$ is reconstructed with the Kalman filter technique Ref. 8, to account for the multiple scattering and energy loss in the detector. The $e^+$ energy scale and resolution are evaluated by fitting the 52.8 MeV kinematic edge of the measured

Michel energy spectrum as shown in Fig.3. The functional form of the fit function is the convolution of the theoretical Michel spectrum and the detector response derived from the Monte Carlo. The latter is well represented by a triple Gaussian. The fit on data returns the following $\sigma$s 374 keV, 1.06 MeV and 2.00 MeV, with fractions of 60 %, 33 % and 7 %, respectively.

### 3.2. *Photon energy $E_\gamma$*

The energy scale and resolution at $E_\gamma = 52.8$ MeV is extracted from the CEX data. The $E_\gamma$ spectrum with 54.9 MeV $\gamma$ from CEX data is shown in Fig.3.
The asymmetry in the line shape is due to conversion in front of the LXe sensitive volume. The resolution depends on the interaction point on the calorimeter surface as well as on the conversion depth ($w$). For deep events ($w > 2$ cm) the average resolution is $\Delta E/E = (5.8 \pm 0.35)\%$ FWHM with a right tail of $\sigma_R = (2.0 \pm 0.15)\%$.
The energy scale is frequently monitored by the 17.67 MeV $\gamma$ from the reactions of CW protons on Li target.
A continuous monitor is available from the $\gamma$ expected spectrum from RMD and $e^+$ annihilation in flight folded with the resolution determined with the $\pi^0$ runs.

### 3.3. *Relative time $t_{e\gamma}$*

The $e^+$ time on the target is obtained by the time measured by the TC corrected by the time-of-flight, as measured by the track-length in the spectrometer. The $\gamma$ time is obtained by the time measured by the LXe corrected by the line-of-flight from the conversion point in the LXe and the $e^+$ extrapolated vertex on the target. In Fig.4, $t_{e\gamma}$ in a normal physics run shows the RMD peak (outside of the blinding-box) clearly visible above the accidental background. The fit for $40 < E_\gamma < 45$ MeV gives $\sigma_{t_{e\gamma}} = (148 \pm 17)$ ps.

### 3.4. *Relative angles $\theta_{e\gamma}$ and $\phi_{e\gamma}$*

The $e^+$ direction and decay vertex are determined by projecting the $e^+$ back to the target. The $\gamma$ direction is defined by linking its conversion point in LXe with the $e^+$ vertex. The $e^+$ angular resolution is evaluated by exploiting double turn tracks, treating each turn as an independent track. The resolutions $\sigma_{\theta_{e\gamma}} = 18$ mrad and $\sigma_{\phi_{e\gamma}} = 10$ mrad are extracted comparing the track parameters at the point of closest approach to the beam-axis. Similarly, the position resolutions are measured to be $\approx 3.2$ mm and $\approx 4.5$ mm in the vertical and horizontal directions.
The position of the $\gamma$ conversion point is reconstructed by using the closest PMT signals. Its resolution is evaluated by Monte Carlo simulation. The average resolutions on the LXe surface are $\approx 5$ mm and in depth $\approx 6$ mm.
The resolution of the relative angles is evaluated by combining the angular and the vertex resolution in the spectrometer and the position resolution in the LXe. The average angular resolutions are $\sigma_{\theta_{e\gamma}} = 21$ mrad and $\sigma_{\phi_{e\gamma}} = 14$ mrad.

## 4. Data analysis

The side-bands outside the blinding-box provides a large sample for defining the analysis algorithms and studying the background. The box is opened after the freezing of the algorithms. The number of $\mu^+ \to e^+\gamma$ events is obtained by a maximum likelihood fit in the analysis region defined as 46 MeV $< E_\gamma <$ 60 MeV, 50 MeV $< E_{e^+} <$ 56 MeV , $|t_{e^+\gamma}| < 1$ ns, $|\theta_{e^+\gamma}| < 100$ mrad and $|\phi_{e^+\gamma}| < 100$ mrad.
A likelihood function L is defined as,

$$\mathcal{L}(N_{sig}, N_{RMD}, N_{BG}) = \frac{N^{N_{obs}} \exp^{-N}}{N_{obs}!} \prod_{i=1}^{N_{obs}} \left[ \frac{N_{sig}}{N} S + \frac{N_{RMD}}{N} R + \frac{N_{BG}}{N} B \right] \quad (1)$$

where $N_{sig}$, $N_{RMD}$ and $N_{BG}$ are the numbers of signal, RMD and accidental background events ($N = N_{sig} + N_{RMD} + N_{BG}$), while $S$, $R$ and $B$ are their probability density functions (PDF). The PDFs are the product of the PDFs for the five observables ($E_\gamma$,$E_e$,$t_{e\gamma}$,$\theta_{e\gamma}$,$\phi_{e\gamma}$) defined by the detector response functions.
The RMD PDF R is the results of folding the theoretical RMD spectrum with the detector response functions. The BG PDF B is the product of the background spectra for the five observables measured in the side bands.
The 90% confidence intervals on $N_{sig}$ and $N_{RMD}$ are determined by the Feldman-Cousins approach Ref 7 that gives an upper limit at 90% C.L. of $N_{sig} < 14.7$ including the systematic error. The largest systematic errors are from the uncertainty of the selection of $\gamma$ pile-up events, the $\gamma$ energy scale, the response function of the $e^+$ energy and the $e^+$ angular resolution.
The upper limit on BR($\mu^+ \to e^+\gamma$) is calculated by normalizing $N_{sig}$ to the number of Michel $e^+$ selected with the same cuts. This technique is independent of the instantaneous beam rate and almost insensitive to $e^+$ acceptance and efficiency

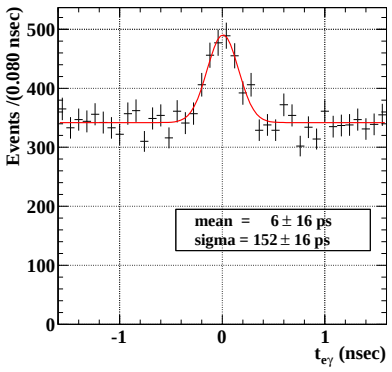


Fig. 4. The distribution of $t_{e\gamma}$ with the RMD peak obtained during physics runs, for $40 < E_\gamma < 45$ MeV. The resolution function used in the analysis accounts for the different energy.

factors related to the spectrometer. The BR can be written as

$$BR(\mu^+ \to e^+\gamma) = \frac{N_{sig}}{N_{e\nu\overline{\nu}}} \times \frac{f^E_{e\nu\overline{\nu}}}{P} \times \frac{\epsilon^{trig}_{e\nu\overline{\nu}}}{\epsilon^{trig}_{e\gamma}} \times \frac{A^{TC}_{e\nu\overline{\nu}}}{A^{TC}_{e\gamma}} \times \frac{\epsilon^{DCH}_{e\nu\overline{\nu}}}{\epsilon^{DCH}_{e\gamma}} \times \frac{1}{A^g_{e\gamma}} \times \frac{1}{\epsilon_{e\gamma}} \qquad (2)$$

where $N_{e\nu\overline{\nu}} = 11414$ is the number of Michel $e^+$ satisfying the cuts; $P = 10^7$ the prescale Michel $e^+$ trigger factor; $f^E_{e\nu\overline{\nu}}$ is the fraction of Michel $e^+$ above 50 MeV; $\frac{\epsilon^{trig}_{e\gamma}}{\epsilon^{trig}_{e\nu\overline{\nu}}} = 0.66 \pm 0.03$ is the ratio of signal-to-Michel efficiencies; $\frac{A^{TC}_{e\gamma}}{A^{TC}_{e\nu\overline{\nu}}} = 1.11 \pm 0.02$ is the ratio of signal-to-Michel DCH-TC matching efficiency; $\frac{\epsilon^{DCH}_{e\gamma}}{\epsilon^{DCH}_{e\nu\overline{\nu}}} = 1.03 \pm 0.005$ is the ratio of signal-to-Michel DCH reconstruction efficiency and acceptance; $A^g_{e\gamma}$ is the geometrical acceptance for signal $\gamma$ provided an accepted $e^+$; $\epsilon_{e\gamma} = 0.63 \pm 0.04$ is the efficiency of $\gamma$ reconstruction and selection criteria.
The limit on $BR(\mu^+ \to e^+\gamma)$ decay including systematic is therefore

$$BR(\mu^+ \to e^+\gamma) \leq 2.8 \times 10^{-11} \qquad (90\% C.L.) \qquad (3)$$

This upper limit can be compared with the experiment sensitivity obtained with MC assuming null signal and numbers from RMD and BG as in the data $1.3 \times 10^{-11}$. The probability to obtain an upper limit greater than Eq.3 is $\approx 5\%$.

## 5. Conclusions

The LFV decay $\mu^+ \to e^+\gamma$ has been searched by the MEG collaboration with a branching ratio sensitivity of $1.3 \times 10^{-11}$, with the data taken during 2008. This sensitivity is comparable with the current branching ratio limit by MEGA BR($\mu^+ \to e^+\gamma$) $\leq 1.2 \times 10^{-11}$ (90% C.L.) Ref 7. An upper limit from a blind likelihood analysis is BR($\mu^+ \to e^+\gamma$) $\leq 2.8 \times 10^{-11}$ (90% C.L.). The problem of low $e^+$ detection efficiency, due to DCH HV trips, has been solved and the DCH worked successfully during the 2009 run. Also the LXe-detector performance has improved resulting in a almost optimal light-yield.

## References

1. T. Schwetz, M. A. Tortola and J. W. F. Valle, *New. J. Phys.* **10**, 11301 (2008).
2. R. Barbieri, L. Hall and A. Strumia , *Nucl. Phys. B* **455** 219 (1995).
3. J. Hisano, D. Nomura and T. Yanagida, *Phys. Lett. B* **437** 351 (1998).
4. M. L. Brooks et al. [MEGA Collaboration], *Phys. Rev. Lett.* **83** 1521 (1999).
5. Y. Kuno and Y. Okada, *Rev. Mod. Phys.* **73** 151 (2001).
6. M. Hildebrandt, *Nucl. Instr. and Meth. A* doi:10.1016/j.nima.2010.02.165.
7. G. J. Feldman and R. D. Cousins, Phys. Rev. D 57, (1998) 3873.
8. R. Frühwirt et al., *Data Analysis Techniques for High Energy Physics*, 2nd edn. (Cambridge University Press, Cambridge, 2000).